Design of a wide field diffractive landscape lens

Dale A. Buralli and G. Michael Morris

The third-order aberrations of a diffractive optical element with paraxial zone spacings are derived as a function of aperture stop position. It is shown that by placing the stop in the front focal plane, coma and astigmatism are identically zero, assuming an infinitely distant object. In addition, since the element is diffractive, the Petzval sum is also zero. Modulation transfer function comparisons with other lenses are given. The correction of spherical aberration using an aspheric plate located in the aperture stop and nonmonochromatic imaging performance are discussed. The distortion of the resulting system is shown to be the proper amount for use as a Fourier transform lens. An estimate for the space–bandwidth product of this Fourier transform system is given.

I. Introduction

The first studies of the aberration properties of diffractive lenses were commonly done by comparing optical path or equivalently phase differences between an object point and image point.[1–4] (The term diffractive lens refers to all optical devices that utilize diffraction in an image forming capability. Familiar diffractive lenses are holographic optical elements, both optically recorded and computer generated, and zone plates.) While giving correct results, these solutions were most often obtained for the special case of the element itself being the limiting aperture (i.e., the aperture stop) or the only element in the system. It is a well-known result of conventional aberration theory that the magnitude of the various aberration coefficients are functions of stop position, and thus the stop position must be taken into account in any general treatment of diffractive lens aberrations.

In 1977 it was shown independently by Sweatt[5] and Kleinhans[6] that a diffractive lens is mathematically equivalent to a thin lens with an infinite refractive index. Using this thin lens analogy, it is possible to apply the results of geometrical optics to diffractive lenses without the need to calculate a special class of formula that applies only to diffractive optics. Calculating the aberrations of optically recorded holographic optical elements with a remote stop was addressed recently by Bobrov and Turkevich[7] and Gan.[8] These authors consider only the case of HOEs formed by the interference of two spherical waves. We are concerned with a more general diffractive lens, which does not correspond to a two-spherical-wave interference pattern.

In particular, for this paper we make use of the so-called stop shift equations for the third-order (Seidel) aberrations in the design of a diffractive landscape lens. We show that a simple system consisting of a single planar diffractive lens with a remote stop can be corrected for coma, astigmatism, and field curvature and thus provide a (monochromatic) imaging performance superior to conventional systems containing several lens elements. In addition to imaging applications, we find that this system is well suited for use as a Fourier transform lens.

II. Seidel Aberrations of Paraxial Diffractive Lens

We are particularly interested in a type of diffractive lens known as a kinoform,[9–11] which has the advantages of being a thin structure with a very high diffraction efficiency. However, the analysis that follows is applicable to any diffractive lens that utilizes a Fresnel zone structure. Also, all the analysis is concerned with only a single diffracted order, since the lens model neglects the possibility of multiple diffracted orders.

The Fresnel (full-period) zones, defined in a plane perpendicular to the optical axis, are defined so that the optical path length from the edge of the mth zone is m design wavelengths (design wavelength = λ_0) longer than the on-axis path length f (which is also the primary focal length of the element).[4] This is the exact specification of the zones for an infinitely distant object. A similar definition can be formed for the case of finite conjugates; we are concerned here with only the infinite conjugates case. Thus the radii of the zones in the x-y plane are given by

$$r_m = \sqrt{2m\lambda_0 f + (m\lambda_0)^2}. \quad (1)$$

In the paraxial region, $f \gg m\lambda_0$, and Eq. (1) can be approximated as

The authors are with University of Rochester, Institute of Optics, Rochester, New York 14627.

Received 10 February 1989.
0003-6935/89/183950-10$02.00/0.

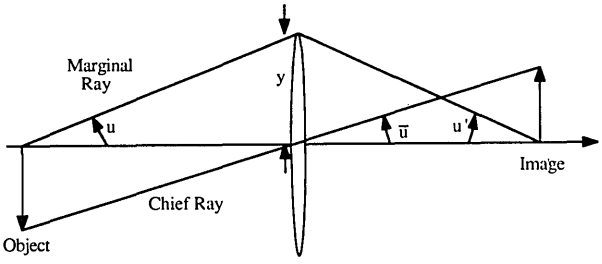

Fig. 1. Pictorial illustration of various paraxial quantities. The numerical value of all symbols is positive with the exception of u'.

$$r_{m,\text{paraxial}} = \sqrt{2m\lambda_0 f}. \tag{2}$$

A diffractive lens with Fresnel zones defined by Eq. (2) for all values of r will be termed a paraxial diffractive lens.

To introduce the notation to be used in the following discussion of the aberrations of a paraxial diffractive lens, we give here one form of the familiar third-order aberrations of a thin lens with stop in contact. The notation and sign convention are those of Welford.[12] The wavefront aberration polynomial has the form (to third order)[13]

$$W(h,\rho,\cos\phi) = \tfrac{1}{8}S_{\mathrm{I}}\rho^4 + \tfrac{1}{2}S_{\mathrm{II}}h\rho^3\cos\phi + \tfrac{1}{2}S_{\mathrm{III}}h^2\rho^2\cos^2\phi + \tfrac{1}{4}(S_{\mathrm{III}} + S_{\mathrm{IV}})h^2\rho^2 + \tfrac{1}{2}S_{\mathrm{V}}h^3\rho\cos\phi. \tag{3}$$

In Eq. (3), h is the normalized object height and ρ and ϕ are the polar pupil coordinates (ρ is the normalized radius coordinate). The Seidel sums (S_{I}–S_{V}) for a thin lens are given by

Spherical aberration:

$$S_{\mathrm{I}} = \frac{y^4\phi^3}{4}\left[\left(\frac{n}{n-1}\right)^2 + \frac{n+2}{n(n-1)^2}B^2 + \frac{4(n+1)}{n(n-1)}BT + \frac{3n+2}{n}T^2\right] + 8Gy^4(\Delta n); \tag{4}$$

Coma:

$$S_{\mathrm{II}} = \frac{-y^2\phi^2 H}{2}\left[\frac{n+1}{n(n-1)}B + \frac{2n+1}{n}T\right]; \tag{5}$$

Astigmatism:

$$S_{\mathrm{III}} = H^2\phi; \tag{6}$$

Petzval curvature of field:

$$S_{\mathrm{IV}} = \frac{H^2\phi}{n}; \tag{7}$$

Distortion:

$$S_{\mathrm{V}} = 0. \tag{8}$$

In Eqs. (4)–(8), n is the index of refraction of the lens, y is the paraxial marginal ray height at the lens, $\phi = (c_1 - c_2)(n-1)$ is the power of the lens (c_1 and c_2 are the curvatures of the two lens surfaces), H is the Lagrange invariant, G is the fourth-order aspheric deformation of a surface (if either or both surfaces are not spherical), Δn is the change in refractive index on passing through the aspheric surface, and B and T are, respectively, the so-called bending and conjugate dimensionless parameters defined as

$$B = \frac{c_1 + c_2}{c_1 - c_2}, \qquad T = \frac{u + u'}{u - u'}. \tag{9}$$

In Eq. (9), u and u' are the paraxial ray angles for the paraxial marginal ray entering and leaving the thin lens. In the following, paraxial quantities that are barred refer to the appropriate quantity for the paraxial chief ray, i.e., the ray that passes through the center of the aperture stop. Figure 1 illustrates the definitions of some of these paraxial quantities for a simple thin lens.

In accord with Refs. 5 and 6, the aberration coefficients for a diffractive lens may be obtained by taking the limit as $n \to \infty$ of Eqs. (4)–(8). For a paraxial diffractive lens with all zones defined by Eq. (2), the aspheric coefficient G is equal to zero for both surfaces of the equivalent thin lens.[6] For the case of an infinitely distant object, the conjugate parameter T is equal to -1. Thus the Seidel sums for a planar, paraxial diffractive lens, object at infinity, stop in contact are

$$S_{\mathrm{I}} = \frac{y^4}{f^3}\left(\frac{\lambda}{\lambda_0}\right)^3, \tag{10}$$

$$S_{\mathrm{II}} = \frac{-y^3\bar{u}}{f^2}\left(\frac{\lambda}{\lambda_0}\right)^2, \tag{11}$$

$$S_{\mathrm{III}} = \frac{y^2\bar{u}^2}{f}\left(\frac{\lambda}{\lambda_0}\right), \tag{12}$$

$$S_{\mathrm{IV}} = 0, \tag{13}$$

$$S_{\mathrm{V}} = 0. \tag{14}$$

In Eqs. (10)–(14) we used the fact that for a diffractive lens utilizing the first diffracted order, the paraxial power is given by

$$\phi(\lambda) = \frac{\lambda}{\lambda_0}\phi_0 = \frac{\lambda}{\lambda_0}\frac{1}{f}, \tag{15}$$

where f is the focal length for $\lambda = \lambda_0$, and at the lens the Lagrange invariant is equal to

$$H = -\bar{u}y, \tag{16}$$

barred quantities referring to paraxial values for the chief ray.

For completeness, we include here the parameters for a nonparaxial diffractive lens that has Fresnel zones defined by Eq. (1). The only change is that the coefficient G of the convex surface of the equivalent lens is equal to[5,6]

$$G = \frac{n^2(\lambda_0)}{8f^3[n(\lambda_0) - 1]^3}. \tag{17}$$

Equation (17) is derived from the well-known result than an infinitely distant on-axis point is stigmatically imaged by an aspheric plano-convex lens, where the convex surface is a hyperbola is eccentricity $\epsilon = n(\lambda_0)$.[14] The coefficient G of Eq. (17) is the fourth-order

aspheric deviation term in the binomial expansion of this hyperbolic surface. Thus, using Eqs. (4) and (17) and taking the limit as $n \to \infty$, the total third-order spherical aberration for this element when used at infinite conjugates is given by

$$S_I = \frac{y^4}{f^3}\left(\frac{\lambda^3 - \lambda\lambda_0^2}{\lambda_0^3}\right). \tag{18}$$

Equation (18) confirms the expected result that at $\lambda = \lambda_0$, this element is free from spherical aberration.

Now we shall consider the effects of moving the stop away from the paraxial diffractive lens. The Seidel sums after the stop shift (denoted by an asterisk) are related to the stop-in-contact sums via the stop-shift equations,[15] i.e.,

$$S_I^* = S_I, \tag{19}$$

$$S_{II}^* = S_{II} + \frac{\bar{y}}{y} S_I, \tag{20}$$

$$S_{III}^* = S_{III} + 2\frac{\bar{y}}{y} S_{II} + \left(\frac{\bar{y}}{y}\right)^2 S_I, \tag{21}$$

$$S_{IV}^* = S_{IV}, \tag{22}$$

$$S_V^* = S_V + \frac{\bar{y}}{y}(3S_{III} + S_{IV}) + 3\left(\frac{\bar{y}}{y}\right)^2 S_{II} + \left(\frac{\bar{y}}{y}\right)^3 S_I. \tag{23}$$

For this simple system of a single element with a remote stop we can write

$$\bar{y} = t\bar{u}, \tag{24}$$

where t is the distance from the stop to the diffractive lens. Due to the large amount of chromatic aberration inherent in diffractive optics [see Eq. (15)], a diffractive lens singlet is limited to monochromatic operation. Since a diffractive kinoform can be designed for operation at any center wavelength, we consider only the case of $\lambda = \lambda_0$. Using Eqs. (10)–(14) and (24) in Eqs. (19)–(23), we find the resultant aberrations with $\lambda = \lambda_0$:

$$S_I^* = \frac{y^4}{f^3}, \tag{25}$$

$$S_{II}^* = \frac{y^3\bar{u}(t-f)}{f^3}, \tag{26}$$

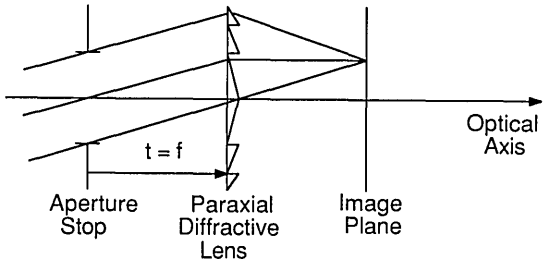

Fig. 2. Layout of telecentric paraxial diffractive lens. The aperture stop for the system is placed in the front focal plane of the lens.

$$S_{III}^* = \frac{y^2\bar{u}^2(t-f)^2}{f^3}, \tag{27}$$

$$S_{IV}^* = 0, \tag{28}$$

$$S_V^* = \frac{y\bar{u}^3 t(3f^2 - 3tf + t^2)}{f^3}. \tag{29}$$

For wavelengths other than the design wavelength, the quantity f in Eqs. (25)–(29) should be replaced by $(\lambda_0/\lambda)f$.

From Eqs. (26) and (27) we see the important result that if the aperture stop is placed in the front focal plane, as shown in the schematic layout of Fig. 2 (i.e., the lens is made telecentric in image space), then $t = f$ and third-order coma and astigmatism are identically zero. Since the Petzval term is also zero, both tangential and sagittal fields are flat. This is in contrast to the glass landscape lens, which has a flat field in only one meridian.[16] Since the remaining third-order spherical aberration limits this diffractive lens to operation at relatively modest apertures, the higher order aberrations are essentially negligible compared with the Seidel aberrations for practical field angles. Thus the third-order aberrations for this telecentric paraxial diffractive lens are

$$S_I^* = \frac{y^4}{f^3}, \tag{30}$$

$$S_{II}^* = S_{III}^* = S_{IV}^* = 0, \tag{31}$$

$$S_V^* = y\bar{u}^3. \tag{32}$$

Equation (31) indicates that the field aberrations of coma, astigmatism, and curvature of field are identically zero for this system, allowing for the imaging of extended objects with little variation in image quality across the field. (Of course, the aperture size is limited by the uncorrected spherical aberration. The tolerance on aperture size is discussed in a following section.) This diffractive lens singlet system exhibits a degree of isoplanatism comparable with refractive systems containing more elements.

As an example of the performance of this diffractive lens system, we compare its performance to a scaled version of a Cooke triplet from Kingslake.[17] The construction parameters for this triplet are given in Table I. Both lenses have a focal length of 50 mm and a relative aperture of $f/5.6$ covering a half field of view of 9.0°. The field of view of the telecentric diffractive lens is limited by the size of the element itself. To avoid vignetting, the semiaperture a of the lens must satisfy

Table I. System Specifications for 50-mm Focal Length Cooke Triplet

Surface	Curvature (mm^{-1})	Thickness (mm)	Glass
1	0.045398	3.000125	SK16
2	−0.008704	7.000116	Air
3 (stop)	−0.058490	1.249783	F4
4	0.065915	7.000371	Air
5	0.010469	1.900544	SK16
6	−0.065708	43.791995	Air

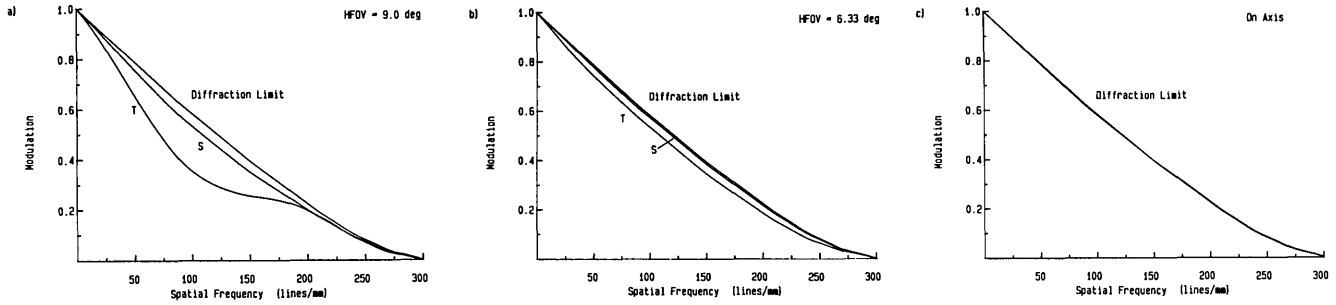

Fig. 3. Modulation transfer functions for $f/5.6$ Cooke triplet; (a) full field (9.0° off-axis); (b) 0.7 field (6.33° off-axis); (c) on-axis. The focal length is 50 mm, and the design wavelength is 0.58756 μm. The triplet system specifications are given in Table I. In each plot, three curves are given—the diffraction limited MTF and the system MTF for tangential and sagittal orientations of the target grating lines.

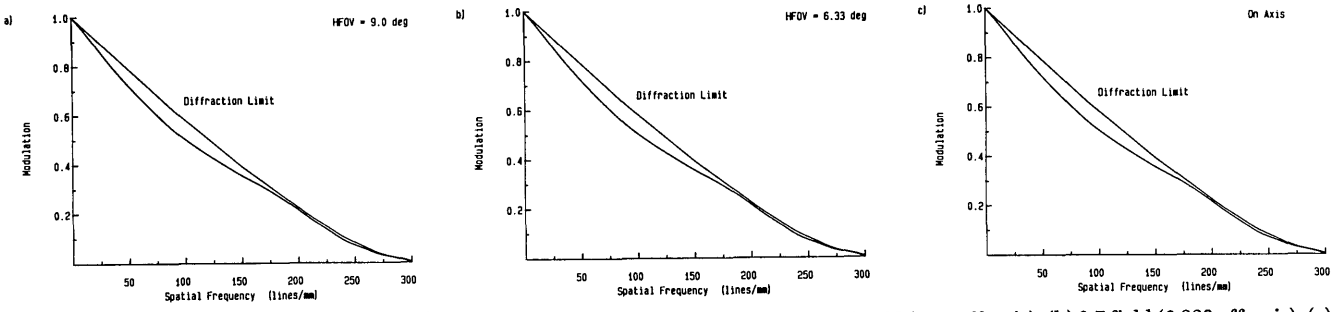

Fig. 4. Modulation transfer functions for $f/5.6$ telecentric paraxial diffractive lens; (a) full field (9.0° off-axis); (b) 0.7 field (6.33° off-axis); (c) on-axis. The focal length is 50 mm, and the design wavelength is 0.58756 μm.

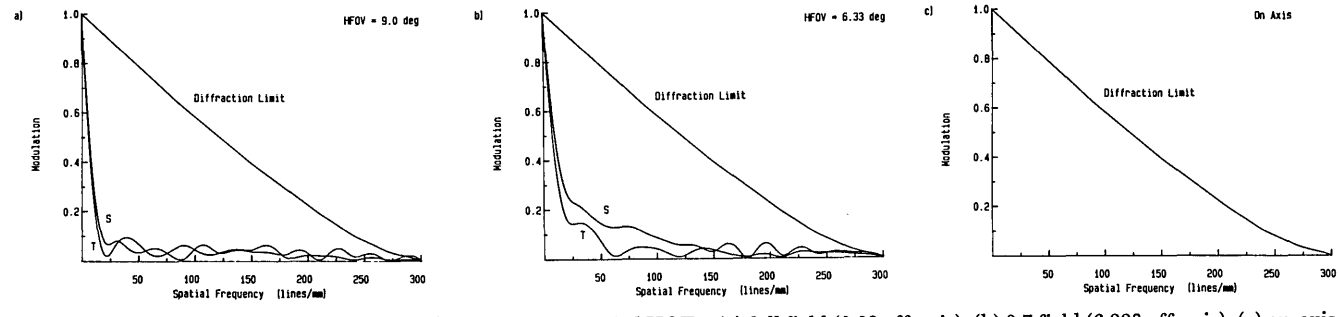

Fig. 5. Modulation transfer functions for $f/5.6$ optically recorded HOE: (a) full field (9.0° off-axis); (b) 0.7 field (6.33° off-axis); (c) on-axis. The focal length is 50 mm, and the design wavelength is 0.58756 μm.

Table II. System Specifications for 50-mm Focal Length Germanium Landscape Lens

Surface	Curvature (mm^{-1})	Thickness (mm)	Glass
1 (stop)	0.000000	43.112883	Air
2	0.004314	4.000020	Ge
3	−0.002376	48.869530	Air

$$y + \bar{y} \le a, \tag{33}$$

or, equivalently for this system,

$$y + f\tan(\theta) \le a. \tag{34}$$

Using Eq. (34) as an equality, we can solve for θ_{max}, the largest unvignetted field angle. Using the relations

$$\frac{f}{2y} = F^{\#}_{\text{system}}, \tag{35}$$

$$\frac{f}{2a} = F^{\#}_{\text{lens}}, \tag{36}$$

we find the result

$$\theta_{max} = \tan^{-1}\left[\frac{1}{2}\left(\frac{1}{F^{\#}_{\text{lens}}} - \frac{1}{F^{\#}_{\text{system}}}\right)\right]. \tag{37}$$

Existing technologies allow for the fabrication of kinoform lenses for use in the visible with relative apertures up to ~$f/2$. Thus an $f/2$ diffractive lens and $f/5.6$ system produce a maximum unvignetted field of view of ~9.0° according to Eq. (37). Figures 3 and 4 show the monochromatic ($\lambda = \lambda_0 = 0.58756\ \mu$m) modulation transfer functions for a Cooke triplet and a telecentric paraxial diffractive lens calculated on-axis, at 0.7 field, and full field. The MTFs were calculated using the optical design program Super-Oslo,[18] and the diffractive lens was modeled as a thin plano-convex (spherical surface) lens[11] of refractive index $n = 10{,}001$. Super-Oslo calculates the MTF by tracing a grid of rays through the system and performing a numerical autocorrelation of the resulting pupil function. We see that the diffractive lens compares favorably with the triplet with respect to MTF. However, not surprisingly, the triplet exhibits superior distortion correction, −0.0898% vs −1.230% at the edge of the field. Examination of the higher order aberrations of the diffractive lens reveals that (other than distortion) the largest field aberration is fifth-order elliptical coma. However, the elliptical coma (in Buchdahl's notation[19] $\mu_7 = -0.792\ \mu$m,$\mu_8 = -0.396\ \mu$m,$\mu_9 = -0.396\ \mu$m) is 1 or 2 orders of magnitude smaller than the third-order spherical aberration ($\sigma_1 = -17.8\ \mu$m).

For comparison, Fig. 5 shows the MTF curves for an optically recorded HOE of the same focal length and aperture. On-axis, the HOE is diffraction limited, as is well known for a HOE formed and used at the same conjugates. At 9.0° off-axis, however, the effects of the uncorrected field aberrations, coma in particular, can be seen in the degradation of the MTF. Optically recorded HOEs can be corrected either for coma, by forming the hologram on a spherical surface,[20] or for astigmatism, by suitable location of the aperture stop.[21]

If the same telecentric paraxial diffractive lens described above is stopped down to a relative aperture of $f/8$, the unvignetted half-field increases to ~10.5°. At this aperture, the spherical aberration is small enough that the lens is essentially diffraction limited over the entire field.

For large field angles, the performance of the lens is limited by the diffraction efficiency of the diffractive lens. Computer calculations of the point spread function for the kinoform described above show that the diffraction efficiency remains >95% (for the design wavelength) for field angles up to 12.5°. These calculations were performed by tracing a polar grid of rays at a specified field angle through the kinoform keeping track of optical path lengths and ray coordinates. The Huygens-Fresnel principle was then used to propagate the diffracted plane wave from the kinoform to the desired image plane. The diffraction integral was calculated numerically, and the squared magnitude was used to determine the intensity of the point spread function. The peak value of the point spread function, normalized to unity for a perfectly spherical diffracted wave (Strehl intensity), found by this procedure is compared to the corresponding value found by using the thin lens model (which assumes 100% efficiency). The ratio gives the diffraction efficiency. (This normalization procedure is necessary to eliminate the effects of lens aberrations in the degradation of the Strehl intensity.) Note that with the kinoform oriented so that the surface relief structure faces the image, at field angles greater than ~15°, total internal reflection of the light incident on the curved facets degrades the diffraction efficiency seriously. This problem may be reduced by orienting the curved facets away from the image, but then the aberrational effects of the finite thickness substrate material must then be considered in determining image quality. In any event, for the range of field angles considered in this paper, orienting the surface relief structure toward the image does not present a problem and is the preferred embodiment.

Since the zone locations are a strong function of wavelength, a diffractive lens designed for use in the thermal IR (λ = 8–12 μm) has many fewer diffracting zones than an element to be used in the visible spectral region and should be easier to fabricate. For example, a 50-mm focal length diffractive lens with a relative aperture of $f/2$ has 2659 diffracting zones if the design wavelength is 0.58756 μm but only 156 zones if $\lambda_0 = 10\ \mu$m. The flat field nature of the telecentric paraxial diffractive lens makes this lens suitable for use with focal plane arrays. Figures 6 and 7 compare the performance of a germanium landscape lens and the diffractive landscape lens at $\lambda_0 = 10\ \mu$m, $f = 50$ mm, $F^{\#}_{\text{system}} = 3.0$, and a half field of view of 10°. The construction parameters for the germanium lens are given in Table II.

III. Correction of Spherical Aberration

As mentioned previously, the aperture size of this telecentric paraxial diffractive lens is limited by the uncorrected spherical aberration. One way to improve the performance of this lens at higher apertures is to insert an appropriately figured aspheric plate in the aperture stop, as shown in Fig. 8. This is formally analogous to the Schmidt camera, which uses an aspheric plate in conjunction with a spherical mirror. Since the aspheric surface is located at the aperture stop, the plate contributes only spherical aberration

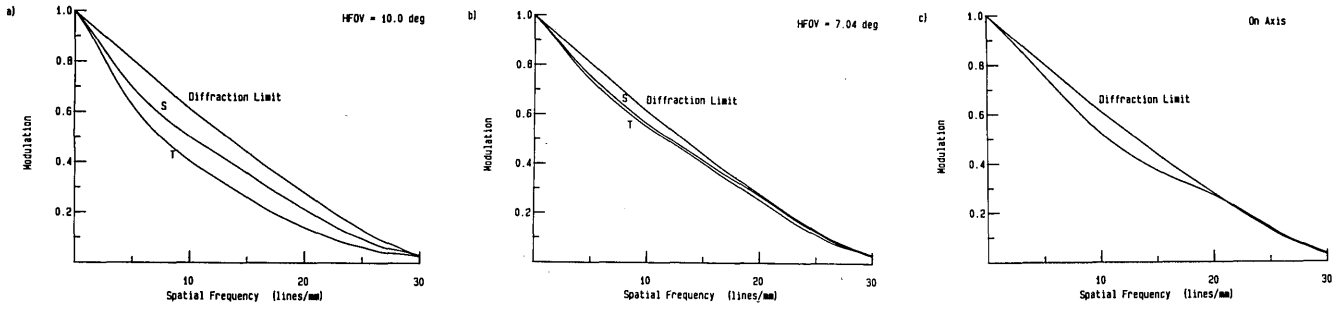

Fig. 6. Modulation transfer functions for $f/3.0$ germanium landscape lens; (a) full field (10.0° off-axis); (b) 0.7 field (7.04° off-axis); (c) on-axis. The focal length is 50 mm, and the design wavelength is 10 μm.

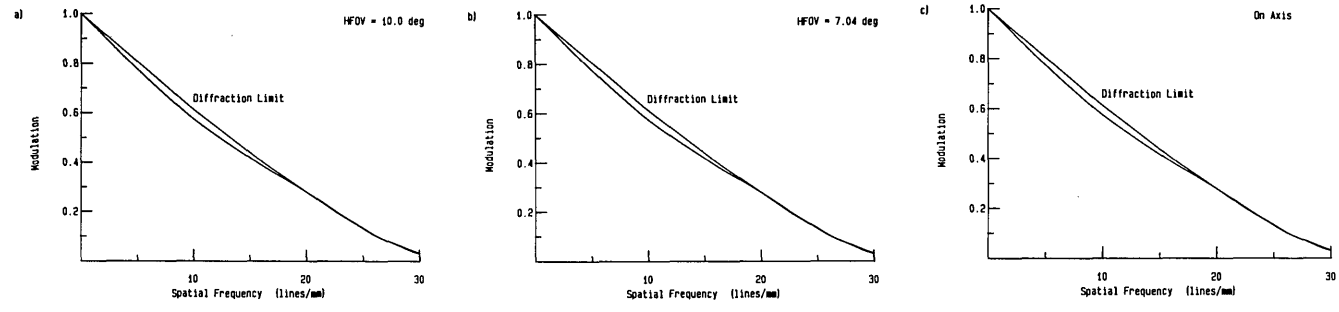

Fig. 7. Modulation transfer functions for $f/3.0$ telecentric paraxial diffractive lens; (a) full field (10.0° off-axis); (b) 0.7 field (7.04° off-axis); (c) on-axis. The focal length is 50 mm, and the design wavelength is 10 μm.

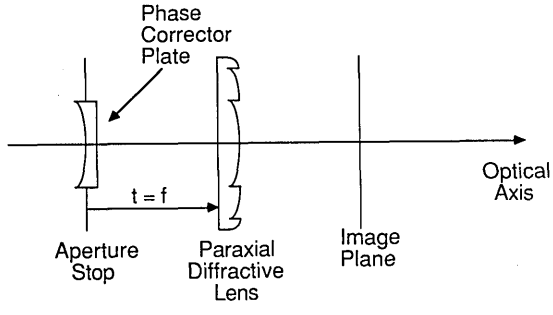

Fig. 8. Layout of the telecentric paraxial diffractive lens with spherical aberration corrected by a Schmidt aspheric plate located in the aperture stop.

(to third order), and thus the correction of the field aberrations is unaffected by this plate. The amount of fourth-order asphericity required is easily determined from the aspheric contributions to the Seidel aberrations. For a refracting surface defined by $z = Gr^4 + \ldots$, the contribution to spherical aberration is given by[22]

$$\delta S_I = 8Gy^4\Delta(n), \tag{38}$$

where $\Delta(n)$ is the change of refractive index on passing through the aspheric surface. For the total spherical aberration to be zero, we require $S_I^* + \delta S_I = 0$. Thus, using Eqs. (30) and (38),

$$\frac{y^4}{f^3} + 8Gy^4\Delta(n) = 0. \tag{39}$$

Solving Eq. (39) for G, we find that the necessary asphericity is

$$G = \frac{-1}{8f^3\Delta(n)}. \tag{40}$$

Of course, for extremely high apertures, higher order asphericities will be necessary to correct fifth and higher order spherical aberration. However, it can be shown that the magnitude of the ratio of third order to fifth order spherical aberration [the aberration polynomial in this case is given by $W(h,\rho,\cos\phi) = W_{040}\,\rho^4 + W_{060}\,\rho^6$] is given by

$$\left|\frac{W_{040}}{W_{060}}\right| = 8(F^{\#}_{\text{system}})^2, \tag{41}$$

so that for practical systems the third order term is dominant by at least an order of magnitude. Also, a theoretical analysis of Schmidt cameras has shown that a fourth-order asphericity is sufficient for relative apertures $>f/3$ and that the location of the aspheric surface on either the front or back surface of the plate affects only higher order aberrations.[23] A telecentric paraxial diffractive lens of 50-mm focal length, $F^{\#}_{\text{system}} = 3.0$, $\lambda_0 = 0.58756$ μm, with an aspheric plate designed according to Eq. (40) in the stop plane is essentially diffraction limited over the unvignetted half-field of 7.0°.

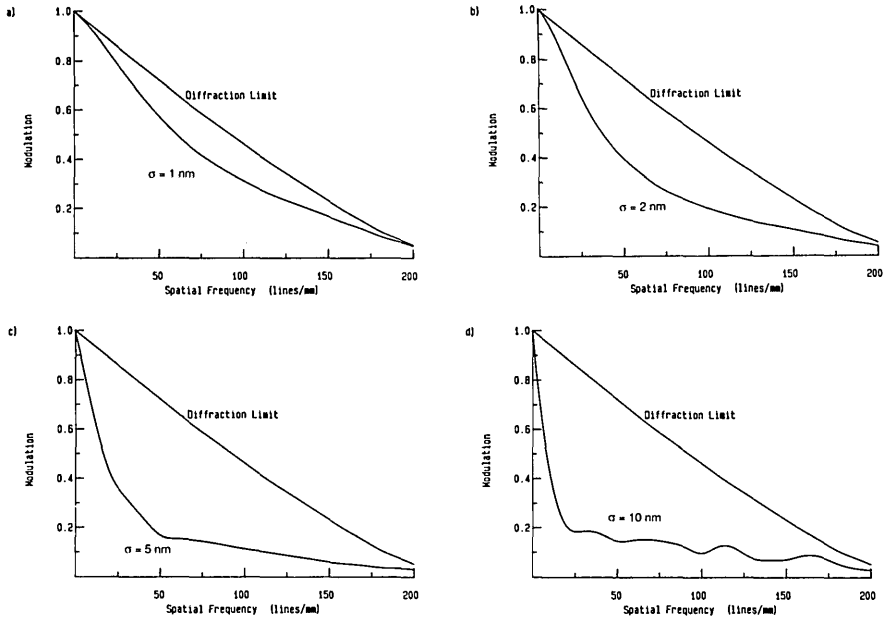

Fig. 9. On-axis polychromatic modulation transfer functions for Gaussian line shapes of various standard deviations σ. The focal length is 50 mm, $\lambda_{peak} = 0.544\ \mu m$, $F^{\#}_{system} = 8$: (a) $\sigma = 1$ nm; (b) $\sigma = 2$ nm; (c) $\sigma = 5$ nm; (d) $\sigma = 10$ nm.

IV. Quasi-Monochromatic Performance

All the analysis to this point has assumed a monochromatic object. In actuality, of course, no physical source is truly monochromatic. To assess the imaging performance of this diffractive lens in quasi-monochromatic light, we used Super-Oslo to calculate polychromatic MTFs for finite bandwidth illumination. Figures 9(a)–(d) show the polychromatic on-axis MTF for Gaussian spectral line shapes of standard deviations of $\sigma = 1, 2, 5$, and 10 nm, respectively. The lens used in these calculations had a 50-mm focal length at the design wavelength (the mean of the Gaussian spectral line) and an f/No. of $F^{\#}_{system} = 8$. The plots clearly show the degradation of performance with increasing linewidth, as would be expected, given the large amount of chromatic aberration. As an illustrative example of typical performance with an actual quasi-monochromatic source, Fig. 10 shows the polychromatic on-axis MTF for a diffractive lens with the spectral weightings assigned according to the relative intensities in the primary yellowish green emission ($\lambda_{peak} = 0.544\ \mu m$) of a $P43$ phosphor.[24] We see that the performance has been degraded slightly due to the finite bandwidth of the source.

V. Paraxial Diffractive Lens as a Fourier Transform Lens

A lens designed for use with an infinitely distant object with the aperture stop in the front focal plane is the configuration necessary for use in a Fourier transform system.[25,26] An additional requirement for this use is that the image height Y formed by the lens should follow the rule $Y = f \sin(\theta)$ rather than $Y = f \tan(\theta)$, which is the rule for a lens that is designed to be distortion free. Image heights proportional to $\sin(\theta)$ ensure a linear relationship between position in the transform plane and spatial frequency in the object for all spatial frequencies. For an image height according to $Y = f \sin(\theta)$, the transverse ray aberration (to third order) should be

$$\epsilon_y = f \sin(\theta) - f \tan(\theta)$$
$$= f\left[\left(\theta - \frac{\theta^3}{6} + \ldots\right) - \left(\theta + \frac{\theta^3}{3} + \ldots\right)\right] = \frac{-1}{2} f\theta^3. \quad (42)$$

Let us now consider the distortion term more carefully. In terms of transverse ray aberration, third-order distortion appears as a term of the form

$$\epsilon_y = \sigma_5 h^3, \quad (43)$$

where ϵ_y is the transverse ray error in the meridional plane, relative to the Gaussian image position, σ_5 is the ray error coefficient, and h is the normalized image height. Since the transverse ray error is related to wavefront aberration via the derivative,[27] there is a relationship between the coefficients σ_5 and S_V, namely,

$$\sigma_5 = \frac{\frac{1}{2}S^*_V}{n'u'}, \quad (44)$$

where n' and u' are the refractive index and paraxial marginal ray angle, respectively, in image space. Thus, using Eqs. (32) and (44) and $n' = 1.0$ and $u' = -y/f$, we find

$$\sigma_5 = \frac{-1}{2} f\bar{u}^3. \quad (45)$$

Since $h = \theta/\theta_{max} = \theta/\bar{u}$, we see that to third order this lens forms an image height according to the rule $Y = f \sin(\theta)$, making it ideally suited for use as a Fourier transform lens.

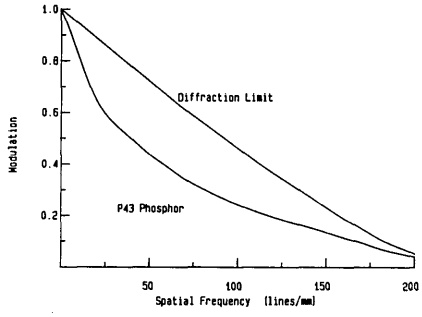

Fig. 10. On-axis polychromatic modulation transfer function for the primary yellowish green emission of a *P*43 phosphor. The focal length is 50 mm, $\lambda_{peak} = 0.544\ \mu m$, $F^{\#}_{system} = 8$.

With regard to imaging with this telecentric diffractive lens, it is interesting to point out that a lens with this amount of distortion will form an image that has uniform irradiance over the entire image plane.[28–30] This is in contrast to the usual $\cos^4$-type irradiance found in well-corrected lenses. For the diffractive lens and Cooke triplet discussed in the previous section, the diffractive lens image has uniform irradiance, while the triplet image irradiance at the edge of the image is decreased by a factor of $\sim\cos^4(9.0°) = 0.952$ from the on-axis value. At larger field angles, the $\cos^4$ losses are much more pronounced.

The uncorrected spherical aberration places a tolerance on the maximum usable aperture for this diffractive lens system. If we use Maréchal's criterion for the maximum allowable wavefront aberration, with the choice of best focal plane,[31] we can tolerate, at most, 0.95λ of spherical aberration. Using Eqs. (3) and (25), we find that the semiaperture y of the aperture stop must satisfy

$$y \le \sqrt[4]{7.6f^3\lambda} \tag{46}$$

for the system not to exceed the Strehl tolerance limit.

A useful quantity for evaluating the performance of a Fourier transform lens is the space–bandwidth product of the lens, which is an estimate of the number of resolvable spots that the system is capable of forming. In one dimension, the object is equal to the diameter of the entrance pupil, which is equal to twice the value of y. The largest spatial frequency F_{max} accepted by the lens is related to the largest diffracted angle θ_{max} by the grating equation, simplified for the case of normally incident illumination and the first diffracted order:

$$\lambda F_{max} = \sin(\theta_{max}). \tag{47}$$

The spatial frequency F is related to a periodicity d by $F = 1/d$. Figure 11 illustrates the parameters in Eq. (47). Using Eq. (37) for θ_{max}, the largest unvignetted spatial frequency is given by

$$F_{max} = \frac{1}{\lambda}\sin\left\{\tan^{-1}\left[\frac{1}{2}\left(\frac{1}{F^{\#}_{lens}} - \frac{1}{F^{\#}_{system}}\right)\right]\right\}. \tag{48}$$

For small angles $\sin(\theta) \approx \tan(\theta)$, and Eq. (48) simplifies to

$$F_{max} = \frac{1}{2\lambda}\left(\frac{1}{F^{\#}_{lens}} - \frac{1}{F^{\#}_{system}}\right). \tag{49}$$

Thus the 1-D space–bandwidth product (for small angles) is given by

$$SBP_{1\text{-}D} = 2yF_{max} = \frac{y}{\lambda}\left(\frac{1}{F^{\#}_{lens}} - \frac{1}{F^{\#}_{system}}\right), \tag{50}$$

where y satisfies Eq. (46). For example, if $f = 250$ mm, $\lambda = 0.58756\ \mu m$, $F^{\#}_{lens} = 3$, and $F^{\#}_{system} = 8.3$ (i.e., $y = 15$ mm), $SBP_{1\text{-}D} \approx 5400$. For comparison, a six-element refractive Fourier transform lens designed by Matsui *et al.*[32] has a 1-D space–bandwidth product of $\sim$5200.

As mentioned above, we allow the nominal focal plane to differ from the paraxial focal plane to offset the aberrational effects of spherical aberration. We can calculate the position of this plane of best focus by finding the focal shift that minimizes the rms wavefront aberration. Considering only defocus and third-order spherical aberration, the wavefront aberration polynomial has the form

$$W(h,\rho,\cos\phi) = W_{020}\rho^2 + W_{040}\rho^4, \tag{51}$$

where W_{020} and W_{040} are the coefficients of defocus and third-order spherical aberration, respectively. It is well known that in this situation W_{rms} is minimized if $W_{020} = -W_{040}$.[33] W_{020} is related to the shift from the Gaussian image plane X via the relation[34]

$$X = \frac{2W_{020}}{n'u'^2}. \tag{52}$$

Using $W_{040} = S_I/8$, the value of S_I given by Eq. (10), the relation $F^{\#}_{system} = -1/2u'$ ($F^{\#}_{system}$ is the f/No. of the system), and Eq. (52), we find that the proper focal shift is

$$X = \frac{-f}{(4F^{\#}_{system})^2}. \tag{53}$$

For the parameters in the example above, $F^{\#}_{system} = 8.3$ and $f = 250$ mm; thus the proper focal shift is $X = -227\ \mu m$. (A negative value for the focal shift means that the best focal plane lies closer to the lens than the paraxial focal plane.) The small amount of higher order spherical aberration will change the position of the optimal focal plane only slightly from the position given by Eq. (53). This paraxially designed profile has

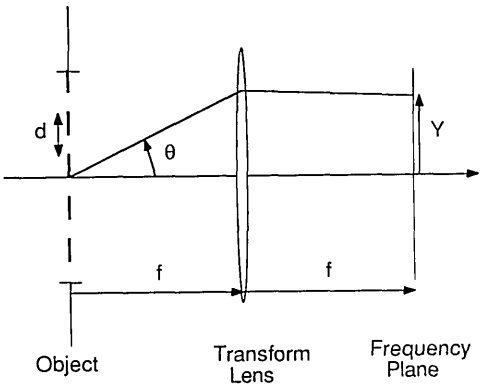

Fig. 11. Optical layout and parameter definitions for an optical Fourier transform. Spatial frequency F is related to object periodicity d by $F = 1/d$. For normally incident illumination, the grating equation reduces to $\sin(\theta) = \lambda/d = \lambda F$.

been previously proposed as a Fourier transform lens.[35] Kedmi and Friesem arrived at their result by minimizing a merit function which was proportional to the difference between the actual diffracted wavefront and the desired wavefront. However, the present analysis reveals more information about why the paraxial diffractive lens performs well in this capacity and also allows for the easier calculation of performance.

We could use the diffractive lens in conjunction with the aspheric plate described in an earlier section to provide a Fourier transform system for objects larger than those allowed by Eq. (46). At first thought, it may seem that increasing the space–bandwidth product is always possible just by increasing y. However, increasing the object size, i.e., decreasing $F^{\#}_{\text{system}}$, will reduce the largest unvignetted field angle accepted by the system (or equivalently $F_{\max}$), according to Eq. (49). Thus we should be able to find an aperture size y so that the space–bandwidth product is maximized. Using Eq. (35), Eq. (50) can be rewritten as

$$\text{SBP}_{1\text{-D}} = \frac{y}{\lambda}\left(\frac{1}{F^{\#}_{\text{lens}}} - \frac{2y}{f}\right). \tag{54}$$

We maximize $\text{SBP}_{1\text{-D}}$ by setting $(d\text{SBP}_{1\text{-D}}/dy) = 0$, recalling that $F^{\#}_{\text{lens}}$ is a constant. The result is

$$y = \frac{f}{4F^{\#}_{\text{lens}}}, \tag{55}$$

or, using Eq. (36),

$$y = a/2. \tag{56}$$

Thus we see that the maximum space–bandwidth product is achieved when the aperture diameter is equal to one-half of the lens diameter.[36] Equation (56) can be equivalently rewritten as

$$F^{\#}_{\text{system}} = 2F^{\#}_{\text{lens}}. \tag{57}$$

Thus far we have assumed that the diffractive lens is being used at the design wavelength λ_0 so that the diffraction efficiency is maximized. However, coma and astigmatism can be made to vanish for any wavelength λ if the stop–lens distance is

$$t(\lambda) = \frac{\lambda_0}{\lambda} f. \tag{58}$$

Obviously the Gaussian focal plane is also a function of wavelength in accordance with Eq. (15). With the stop position dictated by Eq. (58), the distortion coefficient retains the correct value for use as a Fourier transform lens. Thus this single diffractive lens could be used in an optical processing system with more than one laser source as long as the stop position and focal plane can be chosen properly for each wavelength. The diffraction efficiency will decrease from its peak value at λ_0, but for kinoform lenses the diffraction efficiency remains above 80% for a fractional bandwidth $(\Delta\lambda/\lambda_0) > 50\%$.

VI. Summary

We have shown that by utilizing the position of the aperture stop as a variable in a single diffractive lens system, the field aberrations of coma and astigmatism can be made zero. This is possible by allowing the element to have some remaining spherical aberration. Since diffractive lenses also have a zero value for the Petzval sum, this lens has a flat field in both tangential and sagittal meridians. This simple lens can be used to form high quality images over a wider field of view than is possible with conventional optically recorded holographic elements. Since the wavelengths of thermal IR radiation are ~20 times longer than those of visible light, the Fresnel zones of an IR diffractive lens are comparatively wider. This allows for the fabrication of faster elements that could be used at wider field angles, a property that makes this device particularly attractive for use in the IR. For use at larger apertures, a Schmidt camera type aspheric corrector plate could be inserted at the stop to correct the spherical aberration. Since the desired stop position is in the front focal plane and the remaining distortion is such that the image height is proportional to the sine of the incoming field angle, this system forms a simple, yet well-corrected, Fourier transform lens.

References

1. K. Kamiya, "Theory of Fresnel Zone Plate," Sci. Light **12,** 35–49 (1963).
2. R. W. Meier, "Magnification and Third-Order Aberrations in Holography," J. Opt. Soc. Am. **55,** 987–992 (1965).
3. E. B. Champagne, "Nonparaxial Imaging, Magnification, and Aberration Properties in Holography," J. Opt. Soc. Am. **57,** 51–55 (1967).
4. M. Young, "Zone Plates and Their Aberrations," J. Opt. Soc. Am. **62,** 972–976 (1972).
5. W. C. Sweatt, "Describing Holographic and Optical Elements as Lenses," J. Opt. Soc. Am. **67,** 803–808 (1977).
6. W. A. Kleinhans, "Aberrations of Curved Zone Plates and Fresnel Lenses," Appl. Opt. **16,** 1701–1704 (1977).
7. S. T. Bobrov and Yu. G. Turkevich, "Method of Calculating the Wave Aberrations of Complex Holographic Systems," Opt. Spectrosc. USSR **46,** 555–557 (1979).
8. M. A. Gan, "Third-Order Aberrations and the Fundamental Parameters of Axisymmetrical Holographic Elements," Opt. Spectrosc. USSR **47,** 419–422 (1979).
9. L. B. Lesem, P. M. Hirsch, and J. A. Jordan, Jr., "The Kinoform: a New Wavefront Reconstruction Device," IBM J. Res. Dev. **13,** 150–155 (1969).
10. J. A. Jordan, Jr., P. M. Hirsch, L. B. Lesem, and D. L. Van Rooy, "Kinoform Lenses," Appl Opt. **9,** 1883–1887 (1970).
11. D. A. Buralli, G. M. Morris, and J. R. Rogers, "Optical Performance of Holographic Kinoforms," Appl. Opt. **28,** 976–983 (1989).
12. W. T. Welford, *Abberations of Optical Systems* (Hilger, Bristol, 1986), pp. 226–234.
13. Reference 12, pp. 130–140.
14. R. Kingslake, *Lens Design Fundamentals* (Academic, Orlando, FL, 1978), p. 113.
15. Reference 12, pp. 148–152.
16. Reference 14, pp. 211–215.
17. Reference 14, p. 293.
18. Super-Oslo is a trademark of Sinclair Optics, 6780 Palmyra Rd, Fairport, NY 14450.
19. F. D. Cruickshank and G. A. Hills, "Use of Optical Aberration Coefficients in Optical Design," J. Opt. Soc. Am. **50,** 379–387 (1960).
20. W. T. Welford, "Aplanatic Hologram Lenses on Spherical Surfaces," Opt. Commun. **9,** 268–269 (1973); see also W. T. Welford, "Isoplanatism and Holography," Opt. Commun. **8,** 239–243 (1973).
21. R. W. Smith, "A Flat Field Holographic Lens with no First Order Astigmatism," Opt. Commun. **19,** 245–247 (1976); see also R. W. Smith, "Astigmatism Free Holographic Lens Elements," Opt. Commun. **21,** 102–105 (1977); R. W. Smith, "The *s* and *t* Formulae for Holographic Lens Elements," Opt. Commun. **21,** 106–109 (1977).
22. Reference 12, pp. 152–153.
23. E. H. Linfoot, "On the Optics of the Schmidt Camera," Mon. Not. R. Astron. Soc. **109,** 279–297 (1949).
24. Phosphor data taken from "Optical Characteristics of Cathode Ray Tube Screens," TEPAC Publication 116, published by the EIA Tube Engineering Panel Advisory Council (Dec. 1980).
25. B. A. F. Blandford, "A New Lens System for Use in Optical Data-Processing," in *Optical Instruments and Techniques 1969,* J. H. Dickson, Ed. (Oriel, Newcastle upon Tyne, 1970), pp. 435–443.
26. K. von Bieren, "Lens Design for Optical Fourier Transform Systems," Appl. Opt. **10,** 2739–2742 (1971).
27. Reference 12, pp. 93–98.
28. M. Reiss, "The $\cos^4$ Law of Illumination," J. Opt. Soc. Am. **35,** 283–288 (1945).
29. I. C. Gardner, "Validity of the Cosine-Fourth-Power Law of Illumination," J. Res. Natl. Bur. Stand. **39,** 213–219 (1947).
30. M. Reiss, "Notes on the $\cos^4$ Law of Illumination," J. Opt. Soc. Am. **38,** 980–986 (1948).
31. Reference 12, pp. 241–246.
32. Y. Matsui, S. Minami, and S. Yamaguchi, "Fourier Transform Lens System," U.S. Patent 4,189,214 (19 Feb. 1980).
33. Reference 12, p. 244.
34. Reference 12, p. 116.
35. J. Kedmi and A. A. Friesem, "Optimal Holographic Fourier-Transform Lens," Appl. Opt. **23,** 4015–4019 (1984).
36. A. W. Lohmann, "Parallel Interfacing of Integrated Optics with Free-Space Optics," Optik **76,** 53–56 (1987).

The authors would like to acknowledge the support of this research by DARPA, MIT Lincoln Laboratory, and the 3M Co. D. A. Buralli is grateful for the support of the Kodak Fellows Program. Portions of this work were presented as Paper TUM1 at the 1988 Annual Meeting of the Optical Society of America, 30 Oct.–4 Nov. 1988, Santa Clara, CA.